A Shell-Like Induction Electrical Machine

João P. Fernandes, P. Costa Branco

A Shell-Like Induction Electrical Machine

João F. P. Fernandes[1], P. J. Costa Branco[2],
LAETA/IDMEC, Instituto Superior Técnico,
Universidade de Lisboa, Lisbon, Portugal
[1] joao.f.p.fernandes@ist.utl.pt, [2] pbranco@ist.utl.pt

Abstract. This paper proposes to recover the concept of spherical induction electrical machines to conceive a *shell-like* actuator with multi-DOF (Degrees-Of-Freedom). The actuator is formed by a *shell* stator and a spherical rotor. This work contains the feasibility study of that solution when applied as an active joint actuator in assistive devices. Its electromechanical characteristics are first analyzed using an analytic model that includes: the distribution of the magnetic potential vector and thus the components of the magnetic flux density in the airgap due to a sinusoidal current distribution imposed in the stator; the model also shows the induced electromotive forces and associated current density distribution in the rotor; and at last the radial and tangential components of the force density in the rotor. The *shell-like* actuator is concretized as an active joint for assisting movement of the lower leg of a typical 70kg person. Based on its requirements, the joint actuator electromechanical characteristics are analyzed according to its sensitivity to a set of electrical and mechanical variables.

Key words: Electromechanic energy conversion, Electric machines, spherical induction motors, assistive devices.

1 Introduction

Nowadays, multi-DOF motion devices have been mostly formed by a composition of classic electric motors. While today multi-DOF manipulators provide enough accurate motion, the type and number of joints used means a heavy, bulky and expensive structure. Particularly in the area of assistive devices, as active joints [1], and in some industrial applications [2, 3, 4], these manipulators have to be compact, light, with a simple structure and also competitive cost.

This research recovers the concept of classic induction machines to conceive an innovative *shell-like* spherical actuator which allows multi-DOF motion while reducing the complexity of the solution. This work model and analyses its electromechanical characteristics and feasibility as a multi-DOF actuator to operate as an active joint assisting the movement of the lower leg of a typical 70kg person. The key characteristics to be analyzed due to demanded requirements are the amplitude and range of the density forces induced in the rotor and the range of its angular speed.

The paper is divided in the following three steps: *the concept* where the design is explained; *the analytical model* with the statement of its assumptions and computation of its electromechanical characteristics; and in the end the *assistive device* application feasibility and comparison of the analytical and its finite element simulation.

Figures 1 (a) and 1 (b) show the origin of the *shell-like* induction machine concept. The shoulder joint in Fig. 1(a) is multi-axial and possesses the greatest range of motion of any human joint. Meanwhile, the hip joint of the anterior femur in Fig. 1 (b), it presents a shallower shell providing a lower range of motion. A geometrical representation of these joints is shown in Fig. 2. Figure 3 illustrates the conversion of the biomechanical nature to a spherical and *shell-like* induction machine.

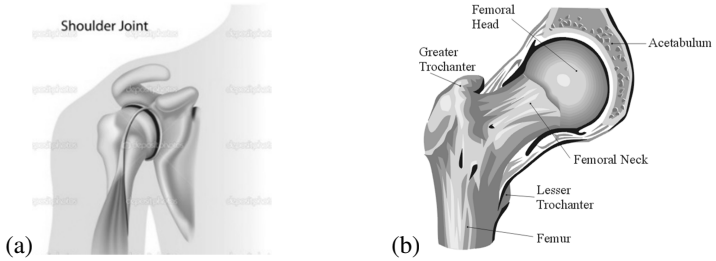

Fig. 1. Main joints of human body. (a) Shoulder joint, (b) hip joint.

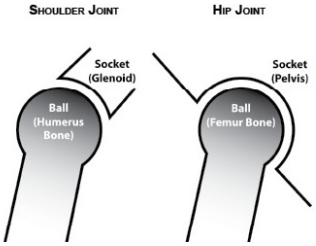

Fig. 2. Large and short range motion due to variable joint socket areas.

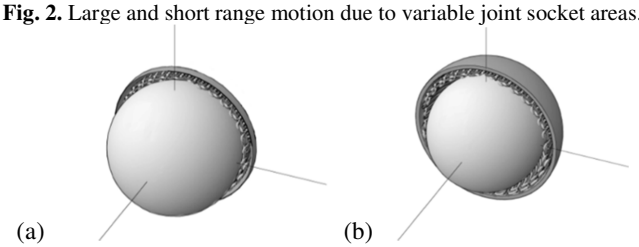

Fig. 3. (a) *Shoulder joint* to a shoulder-like spherical actuator. (b) *Hip joint* to a hip-like spherical actuator

2 Contribution to Collective Awareness Systems

Although the main focus application is in assistive devices, i.e., in *biomedical engineering* systems, its applications can be easily extended to *robotics and integrated manufacturing* systems [2, 3, 4] due to its 3DOF and compact solution, and also used to electric motion devices, as an active wheel [5].

In industrial and motion applications where 3DOF are required, this solution presents a simple control due to its reduced complexity, contributing to the simplification of the *control and decision*, *electronics* and *signal processing systems*.

3 The Concept of a *Shell-Like* Induction Electrical Machine

The *shell-like* design is inspired on the main joints of the human body as shown in Section 1. The stator acts like a socket where the spherical rotor fits, with its periphery defining the range of motion. Figures 2 and 3 illustrated the concept behind the *shell-like* actuator as result of a high range and medium range joints.

The machine uses the same concept of classic induction motors to produce an electromagnetic torque between rotor and stator parts. Figure 4 indicates that the stator is formed by an outer ferromagnetic material layer and an inner layer composed by a distribution set of slotless coils. These will create a travelling magnetic flux density wave that will be commanded to generate an electromagnetic torque in any 3D direction.

The rotor has two layers: the outer one using an electric conductive material and an inner layer of a high magnetic permeability material.

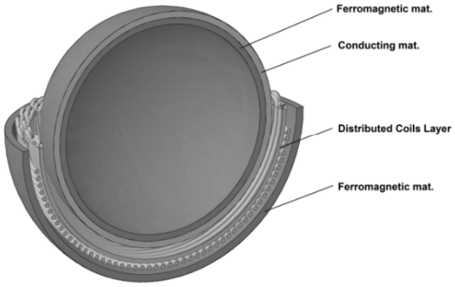

Fig. 4. Shell-like induction machine design.

4 Analytical Model

Figure 5 shows a schematic for the analytical model, which was formulated under the following assumptions: one single homogeneous zone (airgap); a thin current density layer defined as the inner stator surface; a thin electric conducting material layer (σ – electrical conductivity) defined as the outer surface of the rotor; a high permeability ferromagnetic material on the stator and also in the rotor; and negligence of border effects due to the small size of the airgap in relation to the stator length.

To produce an electromagnetic torque it is needed the presence of a travelling wave of electromotive force (EMF) in the rotor. This will be originated by the airgap travelling magnetic wave due to the current density circulating in the stator. The EMF wave is an image of the stator current density being expressed by (1), where k is the wavelength of the stator's EMF (equivalent to the number of poles of the stator):

$$\vec{J}_s = Re\{J_m e^{j(\omega t - k\varphi)} \vec{u}_\theta\} \tag{1}$$

As result the airgap potential vector will be similar to the current density.

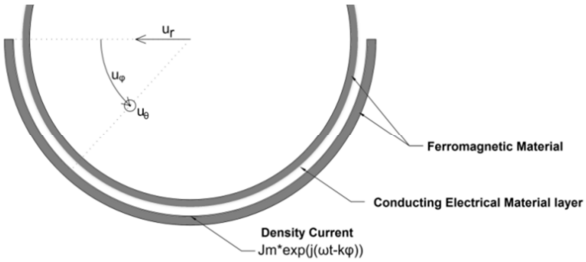

Fig. 5. Cross section of *shell-like* induction machine

The following generic equation defines the potential vector as the composition of two components: a radial dependent component $A(r)$ and a time/space dependent component $e^{j(\omega t-k\varphi)}$:

$$\vec{A}_z = A(r)e^{j(\omega t-k\varphi)}\,\vec{u}_\theta \tag{2}$$

This problem simplifies into the laplacian solution of the radial component $A(r)$. Although initially using spherical coordinates, this *shell-like* design will allow us to change to cylindrical coordinates, simplifying the laplacian solution computation of (2). The following figure illustrates the uniqueness of symmetry around axis -*y* that allows the change of coordinates.

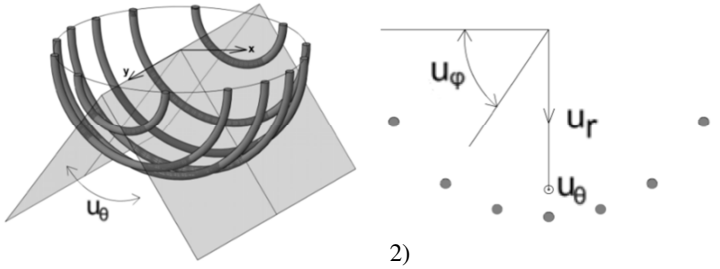

a) 3D representation of one stator coil b) Cross section in 1) and 2)

Fig. 6. Stator's windings geometry in cylindrical coordinates

Therefore the laplacian of potential vector in cylindrical coordinates is defined by:

$$\nabla^2\vec{A}_\theta = \left(\frac{\partial^2 A(r)}{\partial r^2} + \frac{1}{r^2}\frac{\partial^2 A(r)}{\partial \varphi^2} + \frac{\partial^2 A(r)}{\partial \theta^2} + \frac{1}{r}\frac{\partial A(r)}{\partial r}\right)\vec{u}_\theta = 0 \tag{3}$$

Solution of (3) is the typical Cauchy-Euler solution as in (4):

$$\vec{A}_\theta = (C_1 r^k + C_2 r^{-k})e^{j(\omega t-k\varphi)}\,\overrightarrow{u_\theta} \tag{4}$$

Constants C_1 and C_2 in (4) must be defined by two boundary problem conditions. Using the integral form of Ampere's Law, it is possible to establish the relation between magnetic flux density components and density currents on the stator and rotor. These boundary conditions are defined by equations *a* and *b* in (5), and illustrated in Fig. 7(a) and 7(b), respectively.

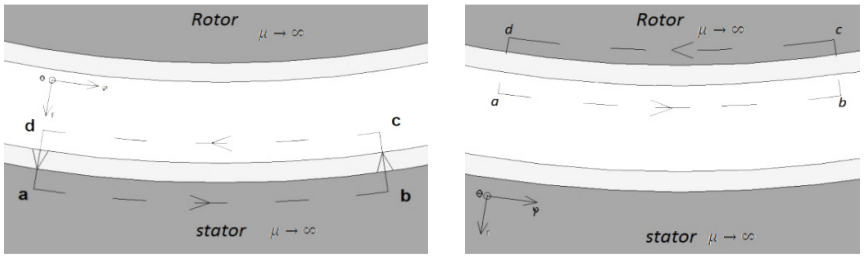

a) b)

Fig. 7. Boundary condition – Ampere's law in the a) stator and b) rotor.

$$a)\ \int_c^d H\,dl = \int_a^b J_S\,\vec{n}d\varphi\ , \qquad b)\ \int_a^b H_\varphi d\varphi = \int_a^b J_i\,\vec{n}d\varphi \tag{5}$$

The stator current density $\vec{J}_s$ is the source for the rotor EMF, resulting in the rotor induced density current $\vec{J}_i$, given by (6), taking in account the electric field $\vec{E}$ and the linear tangential velocity of the rotor, $\vec{V}$.

$$\vec{J}_i = \sigma\left(\vec{E} + \vec{V} \times \vec{B}\right) = \sigma\left(-\frac{\partial \vec{A}_\theta}{\partial t} - \omega_r \frac{\partial \vec{A}_\theta}{\partial \varphi}\right) \tag{6}$$

Defining the slip parameter $\boldsymbol{S = (\omega - k\omega_r)}$, constants $\boldsymbol{C_1}$ and $\boldsymbol{C_2}$ become given by (7) and (8). Term $\boldsymbol{r_r}$ is the radius of the rotor, $\boldsymbol{r_s}$ is the radius of the stator.

$$C_1 = \frac{J_{m_{eq}}\mu_0 {r_s}^{k+1}}{k} \frac{\left(1 + j\frac{\mu_0 \sigma S}{k} r_r\right)}{\left(-{r_r}^{2k} + {r_s}^{2k} + j\frac{\mu_0 \sigma S}{k}({r_r}^{2k} + {r_s}^{2k})\right)} \tag{7}$$

$$C_2 = \frac{J_{m_{eq}}\mu_0 {r_s}^{k+1} {r_r}^{2k}}{k} \frac{\left(1 - j\frac{\mu_0 \sigma S}{k} r_r\right)}{\left(-{r_r}^{2k} + {r_s}^{2k} + j\frac{\mu_0 \sigma S}{k}({r_r}^{2k} + {r_s}^{2k})\right)} \tag{8}$$

4.1 Electromechanical Characteristics

The magnetic flux density is given by the rotational of the potential vector eq. (9). As result, the magnetic flux density presents two components, $\vec{B}_r$ and $\vec{B}_\varphi$, and the induced current only one component, $\vec{J}_\theta$.

$$\vec{B} = \nabla \times \vec{A}_\theta, \qquad \vec{B} = \left(\frac{1}{r}\frac{\partial \vec{A}_\theta}{\partial \varphi}\right)\vec{u}_r + \left(-\frac{\partial \vec{A}_\theta}{\partial r}\right)\vec{u}_\varphi \tag{9}$$

$$\vec{B}_r = -j\frac{k}{r}(C_1 r^k + C_2 r^{-k})e^{j(\omega t - k\varphi)}\vec{u}_r \tag{10}$$

$$\vec{B}_\varphi = -\frac{k}{r}(C_1 r^k - C_2 r^{-k})e^{j(\omega t - k\varphi)}\vec{u}_\varphi \tag{11}$$

$$\vec{J}_i = \sigma\left(-\frac{\partial \vec{A}_\theta}{\partial t} - \omega_r \frac{\partial \vec{A}_\theta}{\partial \varphi}\right) = -j\sigma S(C_1 {r_r}^k + C_2 {r_r}^{-k}) e^{j(\omega t - kd\varphi)} \tag{12}$$

With the magnetic flux density given by (10) and (11) and the induced current density from (12), the magnetic force density in the rotor is computed as in (13). This shows the resultant force density having two components, a radial $\vec{F}_r$ and a tangential one $\vec{F}_\varphi$.

$$\vec{F} = \vec{J}_i \times \vec{B} = \vec{F}_r + \vec{F}_\varphi \tag{13}$$

For motion applications, it is important to analyze the resultant average force density in the rotor and thus the average torque. This can be obtained as shown in (14) taking in account the active surface area of the rotor, its radius and the average force density in (15).

$$\langle T_\varphi \rangle = r_r \iint \langle F_\varphi \rangle \, d\theta \, d\varphi, \qquad \langle T_r \rangle = r_r \iint \langle F_r \rangle \, d\theta \, d\varphi \tag{14}$$

$$\langle F_\varphi \rangle = \frac{1}{2} Re\{\hat{J}_i \hat{B}_r^{\,*}\}, \qquad \langle F_r \rangle = \frac{1}{2} Re\{\hat{J}_i \hat{B}_\varphi^{\,*}\} \tag{15}$$

4.2 Parameters' Sensibility

Figures 8 (a) and (b) show the dependence of the tangential and radial force density in the rotor in function of parameter k, which is the wavelength of stator's EMF. These results were obtained for a 5cm rotor radius with a 2mm thick aluminum material, a 2mm airgap and a stator current density of $6 \times 10^6 A/m^2$ (typical value of current density in electrical machines).

Results show that when increasing the wavelength of EMF (parameter k), both density forces magnitude are reduced, moving the maximum tangential density force to higher values of slip S'. The radial component presents a repulsing force between stator and rotor.

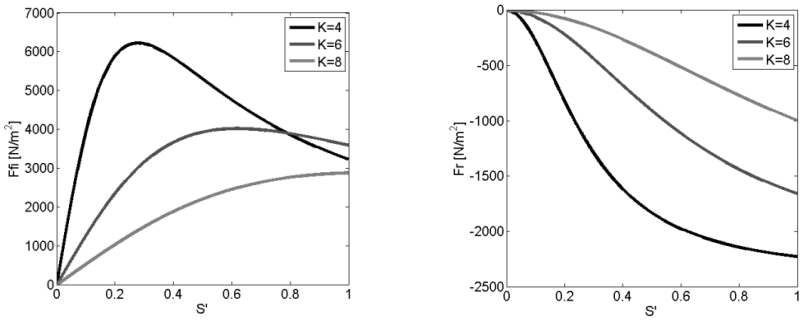

a) b)

Fig. 8. Influence of the EMF's wavelength in the density force components on rotor: (a) tangential component; (b) radial component. $S' = (\omega - k\omega_r)/\omega$.

Figures 9(a) and 9(b) indicate that the change of the rotor's electric conductivity has a similar effect as in classic induction machines. The maximum point of the force will be shifted to higher values of synchronism when decreasing the conductivity.

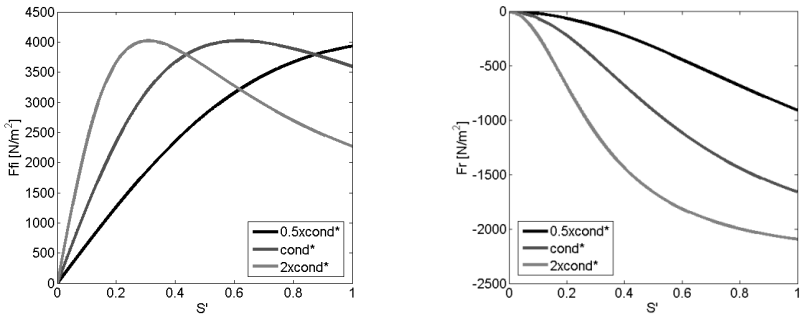

a) b)

Fig. 9. Influence of electric conductivity's material of the rotor in the density force components: (a) tangential component; (b) radial component. $S' = (\omega - k\omega_r)/\omega$.

5 Assistive Device Application

In this section it is analyzed the application of the *shell-like* actuator as an active joint for assistive devices. Application is a device for assistive movement of the lower leg for a typical 70kg person, usually used in orthopedics. Table 1 resumes the specifications of the active joint. For this purpose, the *shell-like* induction motor will have a simple design with a stator shell covering half of the rotor. This design warranties the range of motion in both Sagittal and Coronal planes.

Table 1. Specifications for the orthopedic active joint.

Total weight to lift with a 0.25m distance to the center of mass	2 kg (average lower leg for 70 kg person)
Average linear velocity	3 Km/h [0,83m/s]
Range of Motion for Sagittal plane	[-10° 90°]
Range of Motion for Coronal plane	[-25° 25°]
Rated torque	5 Nm
Range of radius	[2,5 5] cm

To study its feasibility, it was considered a 5cm radius rotor with a 2mm thick aluminum conducting material, a 2mm thick airgap, a 50 Hz stator current density of $6 \times 10^6 \mathrm{A/m^2}$ and k=4. For comparison, our design was simulated in 2D finite element method (FEM) program. FEM results are compared with the analytical solutions. For example, Figure 10 plots the resultant average torque obtained from the analytical model (continuous line) and that one determined using the FEM model (discrete marks).

The maximum torque obtained is about 4 Nm, therefore near to the specified one. The maximum angular velocity corresponds to 3.9m/s (78.5 rad/s), including the average linear velocity of 0.83m/s (16.6 rad/s). This preliminary analysis indicates that the *shell-like* actuator design is capable of be the joint of the orthopedics assistive device.

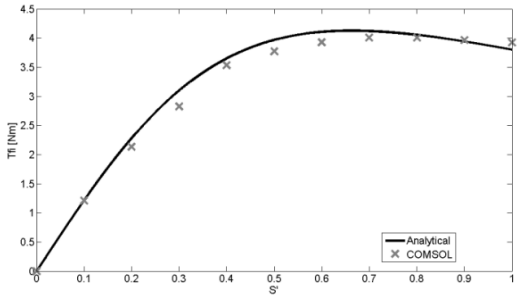

Fig. 10. Tangential component of the torque: analytical and FEM results.

6 Conclusions

The purpose of this paper is to study the feasibility of the shell-like induction machine, especially in assisting devices applications. The combination of the stator shell geometry and distribution of its coils allow a wide range of motion with multi-DOF. By the analysis of the potential vector with a simple model of the machine it was possible to extrapolate its behavior and the amplitude of forces possible for small sizes. Despite the simple model, it was possible to verify the parameter's influence on the main electromechanical characteristics. In addiction the FEM results obtained for a more realistic model, i.e., non-homogeneous geometry with non-simplified structure, were close to the analytical results.

The feasibility study concluded that this machine is capable of originating amplitude of torque needed in an orthopedic assistive device as the proposed leg joint.

Acknowledgements. This work was supported by FCT, through IDMEC, under LAETA Pest-OE/EME/LA0022.

References

1. Ninhuijs, B. van, "Feasibility Study of a Spherical Actuator in an Arm Support", Master graduation paper, Electromechanics and Power Electronics Group, Eindhoven University of Technology, Netherlands, August 2011.
2. T.Suzuki; T.Yano; T.Takatuji: Wafer inspection equipment and system, Japanese Patent No.3641688, 1995.
3. K.M.Lee; H.Son; J.Joni: Concept Development and Design of a Spherical Wheel Motor (SWM), Proc. of 2005 IEEE International Conference on Robotics and Automation, April 2005, pp.3663-3668.
4. H.Kawano; T.Hirahara: Pre-loading Mechanism and Angular Positioning Control Algorithm for Multi-DOF Ultrasonic Motor with a Weight Load, Proc. on 18th International Congress on Acoustic, Mo5.I.2, 2004, pp.I-569-I-572.
5. A.Kagawa; E.Ono; T.Kusakabe; Y.Sakamoto: Absorption of hydrogen by Vanadium-rich V-Ti-Based Alloys, J.Less-Common Met., 172-174, 1991, pp.64-70.